The Importance of Diffusion and Ring Formation in T cell Activation and Synapse Formation

Yves Konigshofer*

* Department of Microbiology and Immunology, Stanford University, Stanford, California 94305, USA

Running title: Simulated Synapses and T cell Activation

Corresponding author:

Dr. Yves Konigshofer
Fairchild D300
299 Campus Drive
Stanford, CA 94305
(650) 725-1170
(650) 725-6757 fax
yvesk@stanford.edu

Abstract

T cell activation by an antigen presenting cell involves the formation of an immunological synapse at the contact area between the cells. This can lead to the clustering of TCR/MHC complexes at the center of the synapse (the c-SMAC) that are surrounded by a ring of LFA-1/ICAM-1 complexes at the periphery of the synapse (the p-SMAC). Here, I present the results of a new adaptable computer simulation that suggest that the formation of transient p-SMAC-like rings is expected when mobile receptors bind to mobile ligands, that the active movement of TCR and CD2 molecules may be towards such rings as opposed to towards the c-SMAC, and that the reason why some TCRs freely diffuse rather than move directly into the synapse may be to prolong TCR signaling.

Introduction

When two cells contact each other, the receptors and ligands on the opposing cells have the opportunity to bind each other in the contact area. This is a frequent process in biological systems and such interactions play an important role in the immune system. In particular, interactions between T cells with antigen presenting cells (APCs) have been the focus of many studies.

When a T cell encounters an APC that presents agonist peptide/MHC complexes, an immunological synapse can form within the contact area between the two cells. This synapse in its mature form usually features TCRs accumulating within the center of the synapse while the adhesion molecule LFA-1 accumulates as a ring around them. Because of its form and presumed function, this central accumulation has been termed the central-supramolecular activation complex (c-SMAC) and the peripheral accumulation has been termed the p-SMAC (1).

Many different molecules have been found to accumulate inside the synapse. Most of these appear to end up inside the c-SMAC and include CD2, CD4, CD8, CD28, Fyn, Lck, and PKCθ (reviewed in (2)). Others, like talin, accumulate inside in p-SMAC and some, like CD4, CD43 and CD45, appear to move away from it. As further studies have explored the distributions of additional molecules during synapse formation, the list of accumulating molecules has grown and raises the question of how and why this accumulation arises in the first place.

While advances in biological assays and microscopy have better defined the processes that give rise to synapse formation, they have also shed light on a remarkable underlying complexity. Synapse formation involves the generation of protein complexes between molecules on opposing cells. These protein complexes may, in turn, affect the formation of other complexes by affecting membrane spacing. Along those lines, interactions between CD2 and CD48/CD58 may promote the formation of nearby similarly-sized complexes between TCRs and MHCs by promoting a 15 nm separation between the membranes of T cells and APCs (3-5). TCR microclusters (6) may appear when TCR and MHC interactions promote the formation of additional nearby TCR/MHC and CD2/CD48 complexes while inhibiting the formation of nearby 40 nm LFA-1/ICAM-1 complexes. Given that the rate at which molecules form complexes is proportional to the product of the concentrations of these molecules, and given that these can vary from cell to cell, the rate of complex formation is expected to vary from cell to cell. While this interconnectedness can eventually give rise to a synapse, it makes it difficult to predict the effects and relative contributions of particular molecules to synapse form and function. For instance, some synapses do not contain a clearly-defined c-SMAC and p-SMAC and, instead, appear to be multifocal in nature where TCRs accumulate at more than one location (7, 8), perhaps due to an inability to coalesce TCR microclusters.

In order to deal with the intrinsic complexity of synapse formation and function, computer simulations have been used. Simulations are built on models, which are themselves dependent on experimental data and assumptions. The simulation of Qi *et al.* (9) suggested that c-SMAC and p-SMAC formation could occur independently of active TCR movement towards the synapse within the normal range of TCR/MHC affinities and was adapted to explain multifocal synapses (10, 11). However, this simulation used a parabolic membrane separation, where the membrane spacing was smallest in the center of the contact area, to drive central clustering. Similar observations were made by Coombs *et al.* using their own simulation (12), but separate simulations designed by Burroughs and Wulfing (13) and Weikl and Lipowsky (14)

concluded that a c-SMAC is unlikely to form without cytoskeletal movement. All of these simulations relied on a planar representation of cells and were limited to a single affinity for TCR and MHC interactions.

Because TCR/MHC interactions have diverse affinities and because T cells and APCs are not flat, I describe here a simulation designed to allow receptors to interact with a variety of ligands that uses a spherical representation of cells and that was expanded to look at a variety of aspects of cell-to-cell contact. This simulation was designed in the JAVA programming language in order to facilitate its use on a variety of operating systems, is available under the GNU General Public License, and can likely be adapted to address a number of additional questions.

Results and Discussion

The Simulation

A simulation was designed in the Java programming language (see Supplemental Material 1) based on a model of two cells that touch each other at a contact area and the algorithms are further described in the Supplemental Materials and Methods. These two cells are represented by one or more spheres, which contain representations of the contact area.

Tracking the interactions of individual molecules presents a computational challenge because each molecule can potentially interact with each other molecule. In order to get around this n-body problem at the expense of some precision, binding was calculated based on the concentrations of molecules in particular regions of the contact area. Different models can be used for dividing the contact area into regions and the contact area can either be part of the sphere (Fig. 1 A) or flat (Fig. 1, B and C). The optimal model is one where the regions are tiled in a brick-like pattern because the borders to adjacent regions are of the same length.

The Monte Carlo method was used to put molecules through iterations where a specified period of time is simulated. Molecules are placed on the spheres and those inside the same region of the contact area can interact with each other. The simulation sequentially puts each molecule through the process illustrated in Fig. 1 D. All rates use first-order rate constants except for the on-rate, k_{on}, which relies on second-order rate constants. In addition, receptor activation occurred after a fixed period of time and molecule synthesis did not rely on a random number to determine whether or not it should take place.

The relative benefits of mobility and affinity of activated LFA-1

Shortly after T cell activation, the affinity of LFA-1 for its ligand, ICAM-1, sharply increases due to a conformational change (15-17) and the diffusion coefficient of LFA-1 increases as well (18). These changes allow T cells to arrest on high endothelial venules (19) and correlate with the appearance of LFA-1/ICAM-1 rings in the p-SMAC during synapse formation (1, 20). The simulation can be used to study equilibrium binding (Supplemental Fig. 1 A), which occurs in two stages (Supplemental Fig. 1 B). First, the molecules inside the contact area have a chance to associate. This occurs in the first 10 seconds, where there is an initial rapid rise in binding and, as shown in Supplemental Fig. 1 C, this is mostly independent of the diffusion coefficient. Thereafter, the rate at which additional molecules bind is dependent on the diffusion coefficients. Given the importance of the rate of diffusion, the simulation was used to determine the absolute and relative effects of increased affinity and increased mobility on the accumulation of LFA-1 and ICAM-1 inside the synapse under optimal and suboptimal binding conditions.

The confinement distance, also known as a confinement region (21, 22), was varied to create optimal and suboptimal conditions. The confinement distance is used to convert membrane densities of proteins into volume concentrations so that three-dimensional association rates can be used. Values as low as 1.2 nm have been reported (20) and such low values may result because the membrane separation next to receptor/ligand complexes may be optimal for the formation of additional receptor/ligand complexes of the same type. On the other hand, if membranes are too close together or too far apart, the formation of additional receptor/ligand complexes may be less likely. In fact, much larger confinement distances, such as 5.8 nm (21) and 1400 nm (23) have been reported and such large confinement distances may occur due to a

disordered orientation of molecules, as would be the case with plate-bound antigen, or if receptor/ligand complexes are ineffective at optimizing membrane spacing.

Reported on- and off-rates were used for interactions between LFA-1 and ICAM-1 (24, 25) and Fig. 2 shows that the increase in affinity of LFA-1 for ICAM-1 after activation was required for their accumulation in the synapse under suboptimal conditions while the increase in mobility of LFA-1 allowed it to accumulate faster. A 2 nm confinement distance led to a significant accumulation of LFA-1 inside the contact area where, after only 4 minutes, over 80% of the LFA-1 outside of the contact area had accumulated inside it. Additionally, even under suboptimal conditions with 20 and 200 nm confinement distances, activated LFA-1 accumulated inside the synapse. At 200 nm, there are 100-fold more complexes between activated LFA-1 and ICAM-1 than when LFA-1 is in its low affinity state. When this form of LFA-1 was allowed to diffuse as if it were activated, it accumulated better than resting slow-moving LFA-1 under optimal conditions, but neither showed a noticeable accumulation when suboptimal conditions were used.

The predicted rapid accumulation of LFA-1 and ICAM-1 is interesting because activated LFA-1 is important in forming and maintaining strong intercellular interactions and because LFA-1 can also act as a costimulatory molecule on T cells (26). The simulation predicts that a large amount of surface LFA-1 and ICAM-1 could become sequestered at the synapse within the first minutes. Given that interactions between helper T cells and APCs can last for hours (27), this may make it difficult for an APC to bind additional T cells if it is already interacting with a T cell – unless, its ICAM levels exceed those of LFA-1 on the first T cell.

The default accumulation pattern of diffusing receptors inside the synapse is a transient ring

The accumulation of molecules inside the synapse has been the subject of early theoretical studies by Bell *et al.* (22) and has been termed “mutual capping” by Kupfer *et al.* (28). Subsequent studies have revealed differences between the accumulation patterns of different molecules within the synapse. Therefore, different binding scenarios were analyzed in order to determine some of the default patterns for diffusion-driven accumulation and Fig. 3 and Supplemental Video 1 clearly illustrate the process of mutual capping where mobile molecules on one cell that have ligands on the other cell accumulate within the synapse.

Fig. 3 A illustrates what happens when mobile molecules on one cell bind to immobile molecules on another cell. This represents the situation when receptors on one cell are anchored to the cytoskeleton while their ligands diffuse freely on another cell and is similar to what was used in Supplemental Fig. 1. The simulation showed a small increase of mobile molecules inside the contact area that, with time, becomes more homogenous over the contact area.

Fig. 3 B illustrates the binding of mobile molecules on one cell to equally mobile molecules on another cell. This represents the usual case where both receptors and their ligands are mobile. When this happens, the diffusion coefficient of the complex is equal to the product of the diffusion coefficients of the receptors and ligands divided by the sum of the diffusion coefficients (29). The simulation showed a strong accumulation of molecules inside the contact area that transitioned through a ring-like pattern and then became relatively well-distributed.

Fig. 3 C illustrates what happens when, unlike in Fig. 3 B, the formation of a complex leads to a greatly-reduced diffusion coefficient for the complex. This represents the case where ligand recognition causes a receptor to become anchored to the cytoskeleton. The simulation showed a strong accumulation of molecules at the edge of the contact area that led to the

formation of a pronounced ring. This was similar to what was reported by Shao *et al.* in their simulation of CD2/CD58 interactions, where there was an accumulation at the edge of the contact area when complexes did not diffuse within the contact area (30).

Membrane models have been very useful in understanding some aspects of synapse formation (9, 12, 13). However, what governs the behavior of membranes inside the synapse is still largely unclear. Here, membrane separation was calculated for each entire region based on the average spacing of complexes and virtual molecules inside of it under the assumption that when a particular receptor/ligand complex forms, the membranes close to that complex are spaced so that the formation of additional complexes of that particular type may be favored and, as more complexes form, this membrane spacing may be reinforced. Virtual molecules act as evenly-distributed immobile struts across the contact area and reinforce a certain membrane separation but are not used for any other computations.

Fig. 3 D illustrates what happens when, unlike in Fig. 3, A – C, the membranes are not spaced optimally for binding. The simulation uses membrane spacings in given regions of the contact area that are the averages of the heights of all complexes in those regions. The on-rate for binding was reduced if the distance spanned by the membranes was not the height of the complex, and movement of complexes between regions was restricted if the membrane spacing at the destination was worse than at the origin. The simulation showed an accumulation that was similar to Fig. 3 B with a slightly more pronounced ring-like transition state.

The conditions used in the simulation shown in Fig. 3 E were very similar to those used in Fig. 3 D except that the movement of complexes between regions was restricted using a two-fold smaller normally-distributed factor. This made it less likely for complexes to move to regions with less-optimal membrane separations. The simulation showed a pronounced punctate accumulation that developed rapidly and was relatively stable. The appearance was similar to what has been reported during microcluster formation (31) and molecules that diffused into the contact area tended to accumulate in clusters at the edge. This suggests that microcluster formation can be caused by suboptimal membrane spacing.

The conditions used in the simulation shown in Fig. 3 F were very similar to those used in Fig. 3 E except that five-fold fewer virtual molecules were used. This led to the formation of persistent channels instead of microclusters. In addition, an outer ring slowly expanded inward as more molecules diffused into the contact area.

Complexes with high affinities accumulated strongly inside the contact area and gave rise to a sharp boundary at the edge of the contact area that could be termed the event horizon of the immunological synapse. As shown in Fig. 3 G, the area just inside the contact area contained more molecules while the area just outside the contact area contained fewer molecules than would have been expected from a random distribution, and this distribution gave rise to a sharp boundary between the contact area and the rest of the cell.

Thus, one can conclude that most complexes should exhibit a transient ring-like distribution at some point during synapse formation and this phenomenon has not been described in other simulations. Importantly, the diffusion-based accumulations do not give rise to preferential accumulations inside the center of the contact area when only single receptor/ligand pairs are simulated and uniform membrane spacings are used.

Directed TCR movement may be towards a ring

While the necessity for active TCR and CD2 movement towards the synapse during simulations of synapse formation has been disputed (9, 12, 13), the central accumulation of both

TCRs and CD2 is dependent on CD2AP when T cells interact with APCs (32, 33). This movement has been determined to occur with a velocity of about $0.05x10^{-6}$ $m \cdot s^{-1}$ (34) and the simulation was used to determine whether or not the central TCR accumulation occurs because these molecules are being drawn towards the center of the synapse. This is important because the data in Fig. 3 failed to show any scenario in which signaling targets for directed TCR movement would form a central accumulation.

During the simulation, each time a molecule moves, a new target is chosen whose location is normally distributed a certain distance from the middle of the contact area. This molecule is then moved closer to this target by a distance dependent on its velocity and the time being simulated. As shown in Fig. 4 A and Supplemental Video 2, when these targets are centered in the middle of the contact area, molecules accumulate rapidly and show an almost immediate central accumulation that leads to a nearly 1000-fold increase in concentration in the center. Given that experimentally-observed accumulations are orders of magnitude lower, it is unlikely that TCRs actively move towards the center of the synapse – at least initially.

On the other hand, when the normal distribution of targets was shifted towards the edge of the contact area, as was the case in Fig. 4 B and Supplemental Video 2, a central accumulation still resulted – but formed gradually and in a less-pronounced way. In this scenario, molecules experienced a slowdown in accumulation once they reached the contact area, which led to the transient formation of a ring. This was very similar to what has been observed when T cell blasts interact with bilayers that contain agonist peptide/MHC complexes and ICAM-1 (31).

This raises the question of why CD2s and TCRs should migrate towards targets that distribute as a ring over the contact area as opposed to the center of the contact area. The answer may be found in Fig. 3 that shows that a ring-shaped transition state is the default configuration for diffusion-based accumulation. During T cell activation, the recognition of one or more agonist peptide/MHC complexes can lead to the activation of LFA-1. LFA-1 is known to signal, and it, or another receptor with a p-SMAC-like accumulation pattern, may be involved in setting targets for the movement of CD2AP. CD2s and TCRs outside the synapse would then move towards the p-SMAC and a sharp concentration gradient of molecules at the event horizon may aid in this process. At the same time, CD2s and TCRs inside the p-SMAC would gradually accumulate close to a point where they are equally likely to move in any direction towards the p-SMAC. This point is the c-SMAC. For this reason, ring-shaped targets were used in this paper when simulating the directed movement of TCRs and CD2s.

Non-stimulatory peptide/MHC complexes can also accumulate within the synapse

While αβ T cell activation only requires the recognition of a small number of agonist peptide/MHC complexes, it has been reported that peptide/MHC complexes that lack the ability to stimulate T cells directly also accumulate within the synapse (35-37). In order to analyze whether such an accumulation should be expected, the location of the different MHC complexes during simulated T cell activation was analyzed.

The simulation was limited to CD2, LFA-1, and αβ TCR on the T cell and CD48, ICAM-1, and MHC on the APC. An average value of about 60,000 MHC class I molecules was reported on splenocytes (38) and, therefore, this number of MHC molecules was simulated, although levels of MHC class II can be an order of magnitude higher. Because the on-rate for TCR/MHC interactions is primarily dependent on interactions between residues on the TCR and MHC while the off-rate is primarily dependent on interactions between residues on the TCR and peptide (39), the on-rates for all TCR/MHC interactions were $2.0x10^{4}$ $M^{-1}s^{-1}$ while off-rates of

0.02 s^{-1}, 0.2 s^{-1} and 2.0 s^{-1} were used for interactions with equal numbers of agonist, partial agonist and null peptides, respectively. The density of CD2 on Jurkat cells was reported to be about 150 molecules/μm^2 (21) and, thus, 50,000 CD2 molecules and 50,000 CD48 molecules were simulated. LFA-1/ICAM-1 interactions used similar values to those in Fig. 2. The activation of LFA-1 may not involve all LFA-1 molecules instantly assuming the high affinity form (40). Therefore, resting LFA-1 molecules were replaced by activated LFA-1 molecules using a first-order rate constant of 0.004 s^{-1}. 50,000 αβ TCRs (20) were simulated and TCR activation was set to occur after 20 s of continuous engagement with MHC while deactivation of unbound activated TCRs was set to occur with a half-life of 2 s, in order to observe how many TCRs were being activated. Given that not all TCRs and CD2 molecules actively move to the synapse, only 80% of them were set to undergo active movement towards the synapse.

Fig. 5 and Supplemental Video 3 show that while only agonist peptide/MHC complexes exhibited a clear accumulation inside the contact area after 120 s, MHCs presenting peptides with off-rates as fast as 2.0 s^{-1} showed subtle accumulations after 600 s when the concentration of TCRs in the middle of the contact area had increased in concentration by 50-fold. At that point, there was also a strong accumulation of CD2 in the middle of the contact area that was surrounded by an LFA-1/ICAM-1 ring.

Antagonist peptides have the ability to inhibit agonist peptide-induced activation when present in excess to agonist peptides and tend to have faster on-rates and much faster off-rates than agonist peptides. Given that null peptide/MHC complexes with fast off-rates can accumulate, albeit subtly, this raises the question of why such complexes do not act as antagonists – especially, when low numbers of agonist peptides are used. In this simulation, the presence of varying amounts of antagonist peptide/MHC complexes did not affect the number of TCRs that became activated or the ability of agonist peptide/MHC complexes to accumulate (data not shown). Thus, antagonist peptides are more likely to act by somehow inhibiting TCR signaling. Perhaps, the action of antagonist peptides is limited to the first few minutes of synapse formation when the presence of CD2 is also predicted to be important (Supplemental Fig. 2). During this time, their faster on-rates may favor their association with TCRs before the membranes are spaced optimally for TCR/MHC interactions.

Freely diffusing TCRs may act to prolong TCR signals

Not all TCRs are anchored to the cytoskeleton and, therefore, not all TCRs actively move towards the synapse. This raises this question of whether or not freely-diffusing TCRs have any biological significance and, thus, extended interactions between T cells and APCs were simulated in the presence of varying amounts of agonist peptide/MHC complexes.

A shown in Fig. 6 A, the presence of 10,000 agonist peptide/MHC complexes led to a strong downregulation of TCR levels. This was accompanied by a decrease in activated TCRs such that after 12 hours, the numbers of activated TCRs were less than when only 100 agonist peptide/MHC complexes were present (Fig. 6 B). When the levels of moving TCRs were analyzed in the presence of 10,000 agonist peptide/MHC complexes (Fig. 6 C), they became very low after only 6 hours. In addition, after this time, the number of activated TCRs was below that obtained with 100 such complexes (Fig. 6 D).

It has been suggested that continued signaling is important in determining the fate of T cells because naïve T cells may require as many as 20 hours of continuous signaling for proliferation (41) and that the c-SMAC, by promoting TCR activation and degradation, may protect against prolonged overstimulation (33). Thus, the levels of agonist peptide/MHC

complexes, the formation of a c-SMAC through active TCR and CD2 movement, and the presence of freely-diffusing TCRs may all help influence the fate of T cells.

Conclusions

This simulation has been useful in revealing a number of novel aspects that may be important in synapse formation and function. For instance, while many studies of synapse formation have focused on the formation and the function of the c-SMAC, simulations to date have not been able to explain the p-SMAC ring, which is predicted here to represent the default accumulation patterns of mobile cell-surface receptors and ligands. Intriguingly, the active movement of TCRs towards, into, and within the synapse is more consistent with their movement towards signals emanating from the p-SMAC than towards signals emanating from the middle of the synapse. Along these lines, the appearance of phosphorylated tyrosines in the p-SMAC has been observed in different experimental settings (42, 43). In addition to the predictions made here, the simulation used in this paper should be adaptable to study many other aspects of cell-to-cell contact in T cells and in any interacting groups of cells.

Materials and Methods

General Equations

The implementation of these equations is further discussed in the Supplemental Materials and Methods. To determine the probability, p, that an event with a first-order rate constant, k, would take place in a given amount of time, t, the following formula was used:

$$p = 1 - e^{-k \times t}$$

A random number between 0 and 1 was then generated and, if this number was smaller than p, then the particular even would take place.

To determine the probability, x/A, that receptor A would be bound to the possible ligands, B_0 *to* B_n, with the second-order rate constants, k_0 *to* k_n, in a given amount of time, t, the following formula was used:

$$\frac{x}{A} = \frac{\left(\sum_{i=1}^{n} B_i k_i\right)^2 \times \left(1 - e^{\frac{t \times \left(A \times \sum_{i=1}^{n} B_i k_i^2 - \left(\sum_{i=1}^{n} B_i k_i\right)^2\right)}{\sum_{i=1}^{n} B_i k_i}}\right)}{\left(\sum_{i=1}^{n} B_i k_i\right)^2 - A \times \left(e^{\frac{t \times \left(A \times \sum_{i=1}^{n} B_i k_i^2 - \left(\sum_{i=1}^{n} B_i k_i\right)^2\right)}{\sum_{i=1}^{n} B_i k_i}} \times \sum_{i=1}^{n} B_i k_i^2\right)}$$

Because of the sequential nature of the simulation, if a receptor did not end up binding to any ligands, these ligands still had the chance to bind to the receptor once it was their turn to undergo binding. Thus, the probability, x/A, was too large when simulating binding sequentially for all molecules. The correct probability, p_{bind}, was obtained as follows:

$$p_{bind} = 1 - \sqrt{1 - \frac{x}{A}}$$

A random number between 0 and 1 was then generated and, if this number was smaller than p_{bind}, then a complex would form. The particular ligand used for the complex was chosen based on the rate of binding to that ligand.

The distance, d_{diff}, that a molecule or complex with the diffusion coefficient, D, diffused in a given amount of time, t, was determined with the following formula where x_a and x_b were random numbers with Gaussian distributions that had standard deviations of 1:

$$d_{diff} = \sqrt{\left(x_a^{\,2} + x_b^{\,2}\right) \times 2 \times D \times t}$$

Diffusion coefficients

Diffusion coefficients of molecules are dependent on the viscosities of the media that surround them. Membrane viscosities are cell-type dependent (44), may be affected by drugs (45), and are highly temperature-dependent (44, 46, 47). When the temperature is increased from a 20°C room temperature to 37°C, diffusion coefficients are expected to increase approximately 3-fold due to a 3-fold decrease in viscosity. Therefore, the diffusion coefficients used in this paper were adjusted from reported values to possible 37°C values.

When simulating T cell interactions with APCs, the following values were used. The αβ TCR is a dimeric molecule that also associates with additional CD3 molecules, which makes its radius inside the membrane rather large. Thus, diffusing αβ TCRs were simulated with diffusion coefficients of 1.8×10^{-14} $m^2 s^{-1}$ (34). A diffusion coefficient of 2.0×10^{-13} $m^2 s^{-1}$ was used (48) for CD2. Both TCRs and CD2 are known to associate with CD2AP (32), which allows them to be moved towards the synapse. The diffusion coefficients of these moving TCRs and CD2s were reduced to 1.0×10^{-15} $m^2 s^{-1}$. MHC molecules have shown considerable variation in their diffusion coefficients (49, 50) but were simulated using diffusion coefficients of 4.0×10^{-13} $m^2 s^{-1}$ and moving and diffusing TCR/MHC complexes used diffusion coefficients of 1.0×10^{-15} and 1.7×10^{-14} $m^2 s^{-1}$, respectively. Because CD48 is GPI-anchored and GPI-anchored molecules have fast diffusion coefficients (50, 51), CD48 molecules were simulated with diffusion coefficients of 8.0×10^{-13} $m^2 s^{-1}$ while moving and diffusing CD2/CD48 complexes used diffusion coefficients of 1.0×10^{-15} and 1.6×10^{-13} $m^2 s^{-1}$, respectively. The diffusion coefficients used for LFA-1 were 2.3×10^{-15} $m^2 s^{-1}$ for the resting state (18) and 4.0×10^{-13} $m^2 s^{-1}$ for the activated state, which is in-line with estimates for transmembrane proteins and was also used for ICAM-1. Rested and activated LFA-1/ICAM-1 complexes had diffusion coefficients of 2.3×10^{-15} and 2.0×10^{-13} $m^2 s^{-1}$, respectively.

Penalizing suboptimal membrane separations

Complex formation and region entry are modeled, in part, using normal distributions. The distance from an optimal value, Δ, and the standard deviation of a normal curve, σ, is used in to determine a *factor* by dividing the value of the normal curve at Δ by the maximal value of the normal curve. This *factor* is then used in further calculations and is given by the following equation:

$$factor = e^{-\frac{1}{2}\left(\frac{\Delta}{\sigma}\right)^2}$$

During complex formation, Δ is the difference between the height of the potential complex and the membrane separation in the region. The on-rate for the formation of the complex is then reduced by multiplying it with the *factor*. This is similar to the approach taken by Qi *et al.* (9).

When an unbound molecule attempts to enter a region where the membranes are spaced closer together than the height of the molecule, or when a complex attempts to enter a region where the membranes do not have the same separation as the height of the complex, Δ is the difference between the height of the complex or unbound molecule and the membrane separation in the region. The *factor* is calculated for both the original and final region and the ratio of these factors influences whether or not the complex or unbound molecule can move to the new region. If not, the simulation will attempt to move the complex or unbound molecule from the original location by a new distance in a new direction.

Acknowledgements

The author wishes to thank his dissertation adviser, Yueh-hsiu Chien, for giving him the time and financial support to conduct the work shown even though it does not feature γδ T cells, the current and past members of the labs of Yueh-hsiu Chien and Mark M. Davis – especially, Cenk Sumen, Lawren Wu, and Johannes Huppa – for helpful discussions, and Mark Davis, Johannes Huppa, Kirk Jensen and Manuel Moertelmaier for critically reading this manuscript.

References

1. Monks, C. R., B. A. Freiberg, H. Kupfer, N. Sciaky, and A. Kupfer. 1998. Three-dimensional segregation of supramolecular activation clusters in T cells. Nature 395:82-86.
2. Huppa, J. B., and M. M. Davis. 2003. T-cell-antigen recognition and the immunological synapse. Nat Rev Immunol 3:973-983.
3. van der Merwe, P. A., P. N. McNamee, E. A. Davies, A. N. Barclay, and S. J. Davis. 1995. Topology of the CD2-CD48 cell-adhesion molecule complex: implications for antigen recognition by T cells. Curr Biol 5:74-84.
4. Choudhuri, K., D. Wiseman, M. H. Brown, K. Gould, and P. A. van der Merwe. 2005. T-cell receptor triggering is critically dependent on the dimensions of its peptide-MHC ligand. Nature 436:578-582.
5. Shaw, A. S., and M. L. Dustin. 1997. Making the T cell receptor go the distance: a topological view of T cell activation. Immunity 6:361-369.
6. Krummel, M. F., M. D. Sjaastad, C. Wulfing, and M. M. Davis. 2000. Differential clustering of CD4 and CD3zeta during T cell recognition. Science 289:1349-1352.
7. Hailman, E., W. R. Burack, A. S. Shaw, M. L. Dustin, and P. M. Allen. 2002. Immature CD4(+)CD8(+) thymocytes form a multifocal immunological synapse with sustained tyrosine phosphorylation. Immunity 16:839-848.
8. Richie, L. I., P. J. Ebert, L. C. Wu, M. F. Krummel, J. J. Owen, and M. M. Davis. 2002. Imaging synapse formation during thymocyte selection: inability of CD3zeta to form a stable central accumulation during negative selection. Immunity 16:595-606.
9. Qi, S. Y., J. T. Groves, and A. K. Chakraborty. 2001. Synaptic pattern formation during cellular recognition. Proc Natl Acad Sci U S A 98:6548-6553.
10. Raychaudhuri, S., A. K. Chakraborty, and M. Kardar. 2003. Effective membrane model of the immunological synapse. Phys Rev Lett 91:208101.
11. Lee, S. J., Y. Hori, and A. K. Chakraborty. 2003. Low T cell receptor expression and thermal fluctuations contribute to formation of dynamic multifocal synapses in thymocytes. Proc Natl Acad Sci U S A 100:4383-4388.
12. Coombs, D., M. Dembo, C. Wofsy, and B. Goldstein. 2004. Equilibrium thermodynamics of cell-cell adhesion mediated by multiple ligand-receptor pairs. Biophys J 86:1408-1423.
13. Burroughs, N. J., and C. Wulfing. 2002. Differential segregation in a cell-cell contact interface: the dynamics of the immunological synapse. Biophys J 83:1784-1796.
14. Weikl, T. R., and R. Lipowsky. 2004. Pattern formation during T-cell adhesion. Biophys J 87:3665-3678.
15. Dustin, M. L., and T. A. Springer. 1989. T-cell receptor cross-linking transiently stimulates adhesiveness through LFA-1. Nature 341:619-624.
16. Moingeon, P. E., J. L. Lucich, C. C. Stebbins, M. A. Recny, B. P. Wallner, S. Koyasu, and E. L. Reinherz. 1991. Complementary roles for CD2 and LFA-1 adhesion pathways during T cell activation. Eur J Immunol 21:605-610.
17. Ma, Q., M. Shimaoka, C. Lu, H. Jing, C. V. Carman, and T. A. Springer. 2002. Activation-induced conformational changes in the I domain region of lymphocyte function-associated antigen 1. J Biol Chem 277:10638-10641.

18. Kucik, D. F., M. L. Dustin, J. M. Miller, and E. J. Brown. 1996. Adhesion-activating phorbol ester increases the mobility of leukocyte integrin LFA-1 in cultured lymphocytes. J Clin Invest 97:2139-2144.
19. Bargatze, R. F., M. A. Jutila, and E. C. Butcher. 1995. Distinct roles of L-selectin and integrins alpha 4 beta 7 and LFA-1 in lymphocyte homing to Peyer's patch-HEV in situ: the multistep model confirmed and refined. Immunity 3:99-108.
20. Grakoui, A., S. K. Bromley, C. Sumen, M. M. Davis, A. S. Shaw, P. M. Allen, and M. L. Dustin. 1999. The immunological synapse: a molecular machine controlling T cell activation. Science 285:221-227.
21. Dustin, M. L., L. M. Ferguson, P. Y. Chan, T. A. Springer, and D. E. Golan. 1996. Visualization of CD2 interaction with LFA-3 and determination of the two-dimensional dissociation constant for adhesion receptors in a contact area. J Cell Biol 132:465-474.
22. Bell, G. I., M. Dembo, and P. Bongrand. 1984. Cell adhesion. Competition between nonspecific repulsion and specific bonding. Biophys J 45:1051-1064.
23. Andersen, P. S., C. Menne, R. A. Mariuzza, C. Geisler, and K. Karjalainen. 2001. A response calculus for immobilized T cell receptor ligands. J Biol Chem 276:49125-49132.
24. Lollo, B. A., K. W. Chan, E. M. Hanson, V. T. Moy, and A. A. Brian. 1993. Direct evidence for two affinity states for lymphocyte function-associated antigen 1 on activated T cells. J Biol Chem 268:21693-21700.
25. Tominaga, Y., Y. Kita, A. Satoh, S. Asai, K. Kato, K. Ishikawa, T. Horiuchi, and T. Takashi. 1998. Affinity and kinetic analysis of the molecular interaction of ICAM-1 and leukocyte function-associated antigen-1. J Immunol 161:4016-4022.
26. Kanner, S. B., L. S. Grosmaire, J. A. Ledbetter, and N. K. Damle. 1993. Beta 2-integrin LFA-1 signaling through phospholipase C-gamma 1 activation. Proc Natl Acad Sci U S A 90:7099-7103.
27. Valitutti, S., S. Muller, M. Cella, E. Padovan, and A. Lanzavecchia. 1995. Serial triggering of many T-cell receptors by a few peptide-MHC complexes. Nature 375:148-151.
28. Kupfer, A., S. J. Singer, C. A. Janeway, Jr., and S. L. Swain. 1987. Coclustering of CD4 (L3T4) molecule with the T-cell receptor is induced by specific direct interaction of helper T cells and antigen-presenting cells. Proc Natl Acad Sci U S A 84:5888-5892.
29. Coombs, D., A. M. Kalergis, S. G. Nathenson, C. Wofsy, and B. Goldstein. 2002. Activated TCRs remain marked for internalization after dissociation from pMHC. Nat Immunol 3:926-931.
30. Shao, J. Y., Y. Yu, and M. L. Dustin. 2005. A model for CD2/CD58-mediated adhesion strengthening. Ann Biomed Eng 33:483-493.
31. Campi, G., R. Varma, and M. L. Dustin. 2005. Actin and agonist MHC-peptide complex-dependent T cell receptor microclusters as scaffolds for signaling. J Exp Med 202:1031-1036.
32. Dustin, M. L., M. W. Olszowy, A. D. Holdorf, J. Li, S. Bromley, N. Desai, P. Widder, F. Rosenberger, P. A. van der Merwe, P. M. Allen, and A. S. Shaw. 1998. A novel adaptor protein orchestrates receptor patterning and cytoskeletal polarity in T-cell contacts. Cell 94:667-677.
33. Lee, K. H., A. R. Dinner, C. Tu, G. Campi, S. Raychaudhuri, R. Varma, T. N. Sims, W. R. Burack, H. Wu, J. Wang, O. Kanagawa, M. Markiewicz, P. M. Allen, M. L. Dustin, A.

K. Chakraborty, and A. S. Shaw. 2003. The immunological synapse balances T cell receptor signaling and degradation. Science 302:1218-1222.
34. Moss, W. C., D. J. Irvine, M. M. Davis, and M. F. Krummel. 2002. Quantifying signaling-induced reorientation of T cell receptors during immunological synapse formation. Proc Natl Acad Sci U S A 99:15024-15029.
35. Wulfing, C., C. Sumen, M. D. Sjaastad, L. C. Wu, M. L. Dustin, and M. M. Davis. 2002. Costimulation and endogenous MHC ligands contribute to T cell recognition. Nat Immunol 3:42-47.
36. Krogsgaard, M., Q. J. Li, C. Sumen, J. B. Huppa, M. Huse, and M. M. Davis. 2005. Agonist/endogenous peptide-MHC heterodimers drive T cell activation and sensitivity. Nature 434:238-243.
37. Irvine, D. J., M. A. Purbhoo, M. Krogsgaard, and M. M. Davis. 2002. Direct observation of ligand recognition by T cells. Nature 419:845-849.
38. Dower, S. K., K. Ozato, and D. M. Segal. 1984. The interaction of monoclonal antibodies with MHC class I antigens on mouse spleen cells. I. Analysis of the mechanism of binding. J Immunol 132:751-758.
39. Wu, L. C., D. S. Tuot, D. S. Lyons, K. C. Garcia, and M. M. Davis. 2002. Two-step binding mechanism for T-cell receptor recognition of peptide MHC. Nature 418:552-556.
40. Lum, A. F., C. E. Green, G. R. Lee, D. E. Staunton, and S. I. Simon. 2002. Dynamic regulation of LFA-1 activation and neutrophil arrest on intercellular adhesion molecule 1 (ICAM-1) in shear flow. J Biol Chem 277:20660-20670.
41. Iezzi, G., K. Karjalainen, and A. Lanzavecchia. 1998. The duration of antigenic stimulation determines the fate of naive and effector T cells. Immunity 8:89-95.
42. Lee, K. H., A. D. Holdorf, M. L. Dustin, A. C. Chan, P. M. Allen, and A. S. Shaw. 2002. T cell receptor signaling precedes immunological synapse formation. Science 295:1539-1542.
43. Mossman, K. D., G. Campi, J. T. Groves, and M. L. Dustin. 2005. Altered TCR signaling from geometrically repatterned immunological synapses. Science 310:1191-1193.
44. Feinstein, M. B., S. M. Fernandez, and R. I. Sha'afi. 1975. Fluidity of natural membranes and phosphatidylserine and ganglioside dispersions. Effect of local anesthetics, cholesterol and protein. Biochim Biophys Acta 413:354-370.
45. Niebylski, C. D., and H. R. Petty. 1991. Cyclosporine A induces an early and transient rigidification of lymphocyte membranes. J Leukoc Biol 49:407-415.
46. Zachariasse, K. A., W. L. Vaz, C. Sotomayor, and W. Kuhnle. 1982. Investigation of human erythrocyte ghost membranes with intramolecular excimer probes. Biochim Biophys Acta 688:323-332.
47. Koyama, T., T. Araiso, and J. Nitta. 1987. Dynamics of membrane structure of frog erythrocyte ghosts measured with a nanosecond fluorometer. Biorheology 24:311-317.
48. Liu, S. J., W. C. Hahn, B. E. Bierer, and D. E. Golan. 1995. Intracellular mediators regulate CD2 lateral diffusion and cytoplasmic Ca2+ mobilization upon CD2-mediated T cell activation. Biophys J 68:459-470.
49. Wade, W. F., J. H. Freed, and M. Edidin. 1989. Translational diffusion of class II major histocompatibility complex molecules is constrained by their cytoplasmic domains. J Cell Biol 109:3325-3331.

50. Vrljic, M., S. Y. Nishimura, S. Brasselet, W. E. Moerner, and H. M. McConnell. 2002. Translational diffusion of individual class II MHC membrane proteins in cells. Biophys J 83:2681-2692.
51. Zhang, F., W. G. Schmidt, Y. Hou, A. F. Williams, and K. Jacobson. 1992. Spontaneous incorporation of the glycosyl-phosphatidylinositol-linked protein Thy-1 into cell membranes. Proc Natl Acad Sci U S A 89:5231-5235.
52. Menne, C., T. Moller Sorensen, V. Siersma, M. von Essen, N. Odum, and C. Geisler. 2002. Endo- and exocytic rate constants for spontaneous and protein kinase C-activated T cell receptor cycling. Eur J Immunol 32:616-626.

Figure Legends

Figure 1: Molecules are affected by various rates, move over the surfaces of spheres, and can interact with other molecules that are inside the same regions of the contact area.

The contact area can either be **(A)** curved or **(B, C)** flat. In order to determine the concentrations of molecules, the contact area is divided into smaller regions, which are indicated by alternating light and dark areas. **(C)** When a flat contact area is tiled using brick-shaped regions, the borders between adjacent regions have the same length. **(D)** Molecules can be in one of many different states and can switch between states using a variety of rate constants (k). Molecules can activate after being bound to particular ligands for a fixed period of time ($t_{activate}$) and can be synthesized at a constant rate.

Figure 2: An analysis of the effects of increased affinity and increased mobility following the activation of LFA-1.

Interactions between 50,000 ICAM-1 and 50,000 activated LFA-1, resting LFA-1 or resting LFA-1 that had the mobility of activated LFA-1 were simulated for 600 s is 0.1 s increments. Confinement distances of 2 nm were used for optimal conditions and 20 and 200 nm were used for suboptimal conditions. **(A)** The percentage of (*solid*) active, (*short dashes*) resting and (*long dashes*) resting with activated mobility LFA-1 that had accumulated inside of the contact area from outside of the contact area at a given time is shown for the different confinement distances. **(B)** The $\log_{10}$ of the relative amount of (*solid*) bound active LFA-1 and (*long dashes*) bound resting with activated mobility LFA-1 compared to bound resting LFA-1 is shown for the different confinement distances. Cells were represented by spheres with 5 μm radii and the contact area had a radius of 4 μm. Membranes were spaced 40 nm apart, which was also the height of the complex between 19 nm ICAM-1 and 21 nm LFA-1. The on- and off-rates for interactions with activated LFA-1 were 2.0×10^5 $M^{-1}s^{-1}$ and 0.1 s^{-1}, respectively. The on- and off-rates for interactions with resting LFA-1 were 3.67×10^2 $M^{-1}s^{-1}$ and 0.033 s^{-1}, respectively. Each simulation was repeated three times.

Figure 3: Diffusion can lead to different accumulation patterns under different conditions and often leads to ring formation.

The binding of 150,000 19 nm receptors to 150,000 21 nm ligands was simulated in 0.1 s increments under different conditions. The locations of the ligand are shown at the start of the simulation, after 100 s and after 600 s. In addition, the ratios of observed to expected ligands found from the inside to the outside of the contact area are shown at (*thin black*) 0, (*medium black*) 100, (*25% gray*) 200, (*40% gray*) 300, (*50% gray*) 400, (*80% gray*) 500 and (*thick black*) 600 s. Cells were represented by spheres with 5 μm radii and the flat contact area had a radius of 4 μm. The on-rate was 2.0×10^5 $M^{-1}s^{-1}$, the off-rate was 0.1 s^{-1}, and the confinement distance was 2 nm. **(A)** Binding to an immobile receptor was simulated. Membranes were spaced 40 nm apart. The receptors and their complexes with ligands were immobile while free ligands had diffusion coefficients of 3.0×10^{-14} m^2s^{-1}. **(B)** Binding to a mobile receptor was simulated. The receptors now also had diffusion coefficients of 3.0×10^{-14} m^2s^{-1} while complexes had diffusion coefficients of 1.5×10^{-14} m^2s^{-1}. **(C)** Binding-induced receptor arrest was simulated. Free receptors and ligands had diffusion coefficients of 3.0×10^{-14} m^2s^{-1} while complexes had diffusion coefficients of 0.5×10^{-15} m^2s^{-1}. **(D)** The effects of suboptimal membrane separation were simulated. 100,000 virtual molecules led to a 20 instead of 40 nm starting membrane separation.

The σ for the normal curve penalizing the on-rate was 10 nm. The σ for the normal curve penalizing movement between regions was 10 nm for the 40 nm complexes and 5.25 nm for the 21 nm ligands. **(E)** The effects of a decreased σ on the movement of complexes were simulated. The σ for the normal curve penalizing the movement of complexes between regions was reduced to 5 nm. **(F)** The effects of increasing the contribution of receptor/ligand complexes to the membrane separation were simulated. The numbers of virtual molecules were reduced to 20,000. **(G)** A curved instead of a flat contact area was used. Log10s of ratios of observed to expected ligands for (*thin black*) starting conditions and after 600 s simulations that were similar to (*light gray*) **(A)**, (*medium gray*) **(B)** and (*thick black*) **(C)** are shown from the middle of the contact area to the opposite end of the sphere.

Figure 4: TCRs and CD2s may be actively moving towards the periphery, instead of the center, of the synapse.

150,000 molecules that moved towards the contact area with a velocity of 0.05×10^{-6} $m \cdot s^{-1}$ and had diffusion coefficients of 1.0×10^{-15} $m^2 s^{-1}$ were simulated for 600 s in 0.1 s increments. Cells were represented by spheres with 5 μm radii and contact areas had radii of 4 μm and were divided into 20x20 grids of square regions that were each allowed to contain up to 6250 molecules. **(A)** The locations of molecules and the ratios of observed to expected molecules that are found from the inside to the outside of a flat contact are shown after (*thin black*) 0, (*25% gray*) 120, (*50% gray*) 240 and (*thick black*) 480 s of movement. Movement occurred towards targets that were centered at the middle of the contact area and normally distributed with a σ of 0.1×10^{-6} μm. Because there was a limit to how many molecules could be physically packed into a given region, later timepoints showed a jagged accumulation. **(B)** The simulations in **(A)** were repeated except that movement occurred towards targets that were centered 3.5 μm away from the middle of the contact area and were normally distributed with a σ of 0.5 μm. Each simulation was repeated three times.

Figure 5: The accumulation of TCRs inside the contact area leads to the accumulation of MHC complexes with diverse affinities.

The locations of TCRs, three different MHC complexes, CD2, CD48, ICAM-1 and LFA-1 at 0, 120 and 600 s timepoints are shown. In addition, the ratios of observed to expected (*thin black*) TCRs and MHC complexes with off-rates of (*thick black*) 0.02, (*50% gray*) 0.02 and (*25% gray*) 2.0 s^{-1} that are found from the inside to the outside of the contact area are shown at these timepoints.

Cells were represented by spheres with 5 μm radii and the flat contact area had a radius of 4 μm. Membranes were spaced 30 nm apart using 13,000 virtual molecules. The contact area was divided into a 20x10 grid of brick-shaped regions that were each allowed to contain 6250 molecules. 600 s were simulated in 0.01 s increments. TCR and CD2 movement occurred towards targets that were centered 3.5 μm away from the middle of the 4 μm contact area and were normally distributed with a σ of 0.5 μm.

50,000 7 nm TCRs were simulated, of which 80% moved with a velocity of 0.05×10^{-6} $m \cdot s^{-1}$ and 87% were found on the surface at the start. For region entry, the σ for unbound moving and diffusing TCRs were 40 and 3 nm, respectively. TCRs activated after being bound continuously for 20 s. External unbound TCRs deactivated with a rate constant of 0.34657 s^{-1} and internal TCRs deactivated with a rate constant of 0.01155 s^{-1}. Resting and activated TCRs were internalized with rate constants of 0.25×10^{-3} and 1.97×10^{-3} s^{-1}, respectively (52). Internal

activated TCRs were degraded with a rate constant of 0.1 s^{-1}. One TCR was synthesized per minute, and TCRs were externalized towards the middle of the contact area with σ of 5 μm and a rate constant of 0.00167 s^{-1}. TCRs interacted with 60,000 7 nm MHC complexes to form 15 nm TCR/MHC complexes. These were equally split into three types and TCR/MHC interactions used a confinement distance of 2 nm, an on-rate of $2.0x10^3$ $M^{-1}s^{-1}$ with a σ of 8 nm, and off-rates of 2.0, 0.2 or 0.02 s^{-1}. For region entry, the σ for unbound MHC complexes and for moving and diffusing TCR/MHC complexes were 3, 40 and 3 nm, respectively. When present, 50,000 7 nm CD2 were simulated, of which 80% moved with a velocity of $0.05x10^{-6}$ $m{\cdot}s^{-1}$. For region entry, the σ for unbound moving and diffusing CD2 were 40 and 3 nm, respectively. CD2 interacted with 50,000 7 nm CD48 to form 15 nm CD2/CD48 complexes. CD2/CD48 interactions used a confinement distance of 2 nm, an on-rate of $1.0x10^5$ $M^{-1}s^{-1}$ with a σ of 8 nm and an off-rates of 6.0 s^{-1}. For region entry, the σ for unbound CD48 and for moving and diffusing CD2/CD48 complexes were 3, 40 and 3 nm, respectively. CD2 movement occurred towards targets that were centered 3.5 μm away from the middle of the 4 μm contact area and were normally distributed with a σ of 0.5 μm.

100,000 resting and 100,000 activated 21 nm were simulated. Resting LFA-1 was removed using a rate-constant of 0.004 s^{-1}. Activated LFA-1 was added at random locations using a rate constant of 0.004 s^{-1}. For region entry, the σ for LFA-1 was 3 nm. LFA-1 interacted with 100,000 19 nm ICAM-1 to form 40 nm LFA-1/ICAM-1 complexes. LFA-1/ICAM-1 interactions used a confinement distance of 2 nm. Resting and activated LFA-1/ICAM-1 interactions used on-rates of 367 and $2.0x10^5$ $M^{-1}s^{-1}$ with a σ of 8 nm and off-rates of 0.033 and 0.1 s^{-1}, respectively. For region entry, the σ for unbound ICAM-1 and for resting and activated LFA-1/ICAM-1 complexes were 3 nm.

Figure 6: Diffusing, as opposed to moving, TCRs may act to prolong the presence of active TCRs on the surface.

Numbers of total surface TCRs, total active surface TCRs, moving surface TCRs and moving active surface TCRs are shown over 24 hours. Similar conditions to Fig. 7 were used with the following modifications. The contact area was divided into a 5x5 grid of square regions that were each allowed to contain 104,000 molecules. 24 hours were simulated in 10 s intervals. TCRs deactivated with a rate constant of 0.034657 s^{-1}. A total of 60,000 MHC complexes were present where 1,000 partial agonist-presenting MHCs dissociated from TCRs with off-rates of 0.2 s^{-1}, either (*thin black*) 0, (*25% gray*) 100, (*50% gray*) 1000 or (*thick black*) 10,000 agonist-presenting MHCs dissociated from TCRs with off-rates of 0.02 s^{-1}, and the remaining MHCs dissociated from TCRs with off-rates of 2.0 s^{-1}.

Figure 1

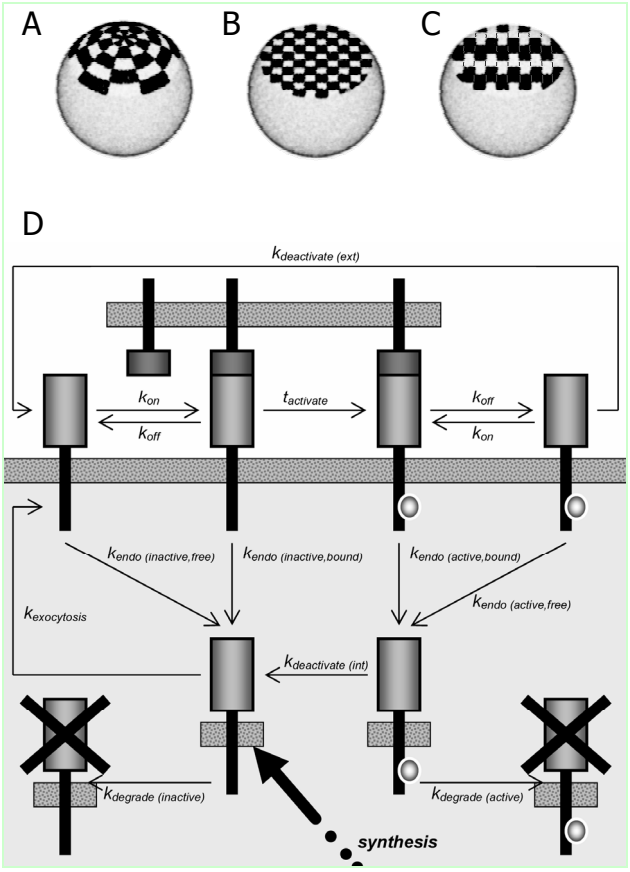
A
B
C
D
$k_{deactivate\ (ext)}$
k_{on}
k_{off}
$t_{activate}$
k_{off}
k_{on}
$k_{endo\ (inactive,free)}$
$k_{endo\ (inactive,bound)}$
$k_{endo\ (active,bound)}$
$k_{endo\ (active,free)}$
$k_{exocytosis}$
$k_{deactivate\ (int)}$
$k_{degrade\ (inactive)}$
$k_{degrade\ (active)}$
synthesis

Figure 2

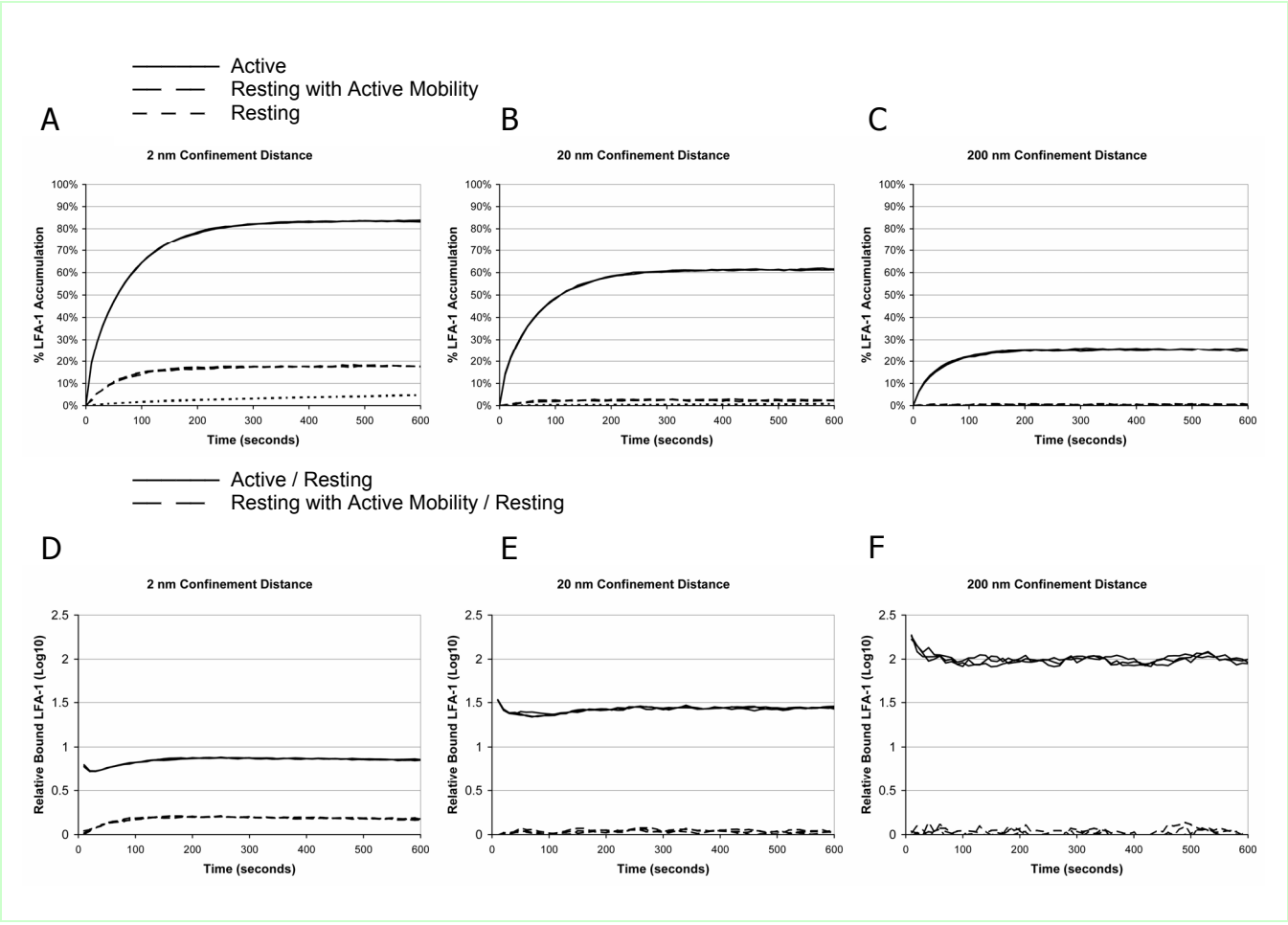
Active
Resting with Active Mobility
Resting
A
B
C
2 nm Confinement Distance
20 nm Confinement Distance
200 nm Confinement Distance
% LFA-1 Accumulation
Time (seconds)
Active / Resting
Resting with Active Mobility / Resting
D
E
F
Relative Bound LFA-1 (Log10)

Figure 3

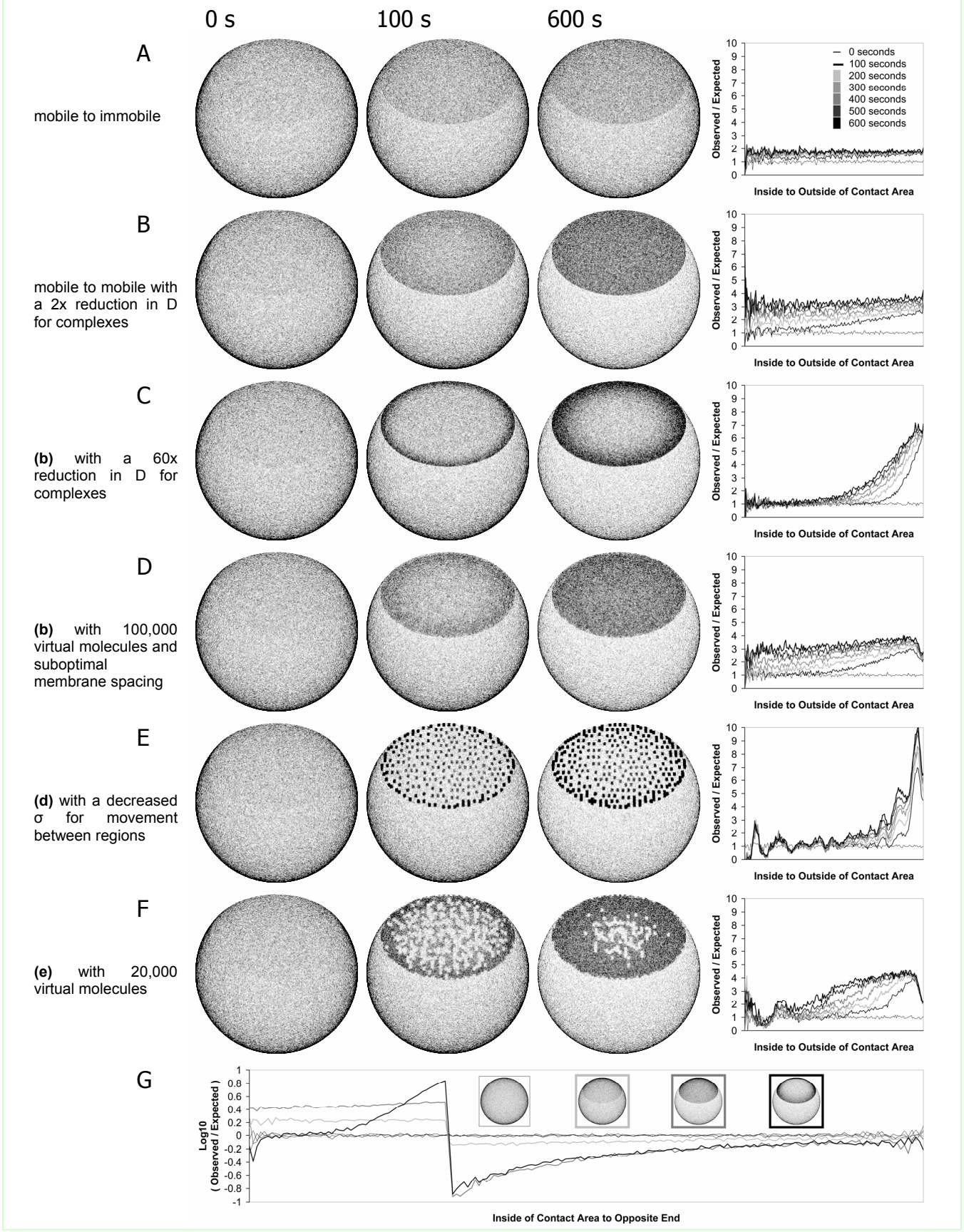
0 s
100 s
600 s
A
mobile to immobile
B
mobile to mobile with a 2x reduction in D for complexes
C
(b) with a 60x reduction in D for complexes
D
(b) with 100,000 virtual molecules and suboptimal membrane spacing
E
(d) with a decreased σ for movement between regions
F
(e) with 20,000 virtual molecules
G
0 seconds
100 seconds
200 seconds
300 seconds
400 seconds
500 seconds
600 seconds
Observed / Expected
Inside to Outside of Contact Area
Log10 (Observed / Expected)
Inside of Contact Area to Opposite End

Figure 4

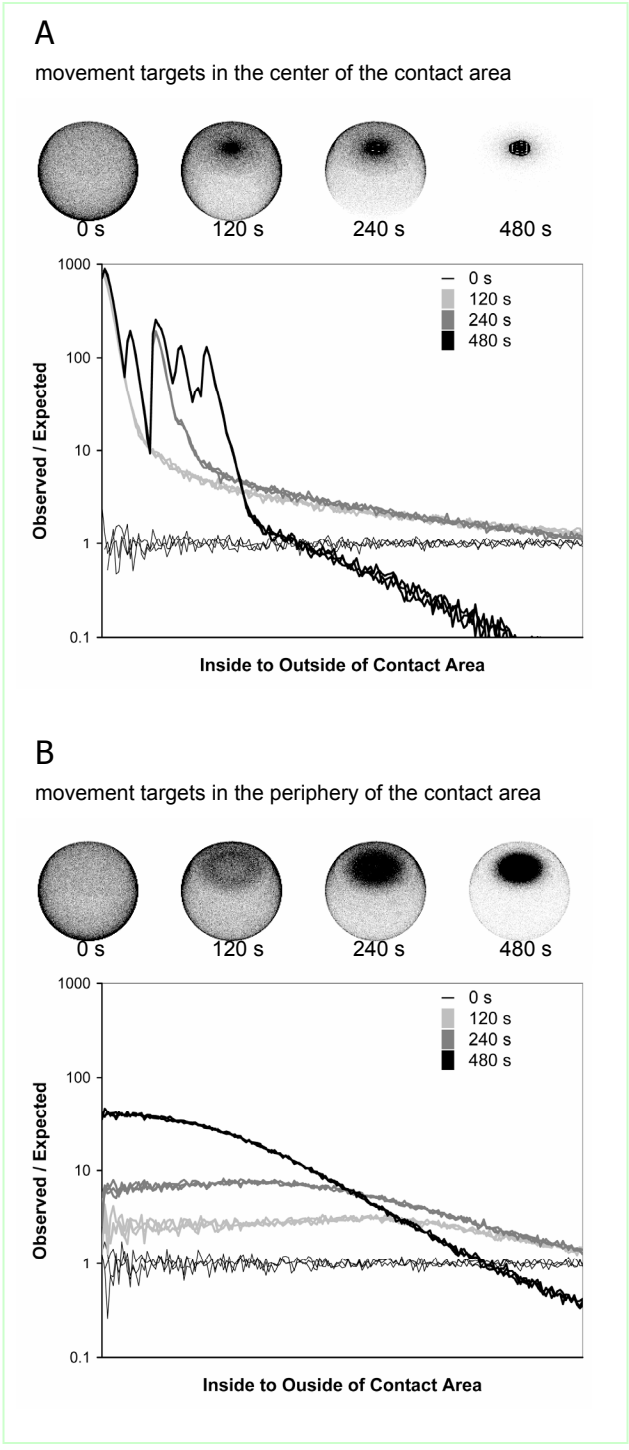
A
movement targets in the center of the contact area
0 s
120 s
240 s
480 s
1000
100
10
1
0.1
Observed / Expected
0 s
120 s
240 s
480 s
Inside to Outside of Contact Area
B
movement targets in the periphery of the contact area
0 s
120 s
240 s
480 s
1000
100
10
1
0.1
Observed / Expected
0 s
120 s
240 s
480 s
Inside to Ouside of Contact Area

Figure 5

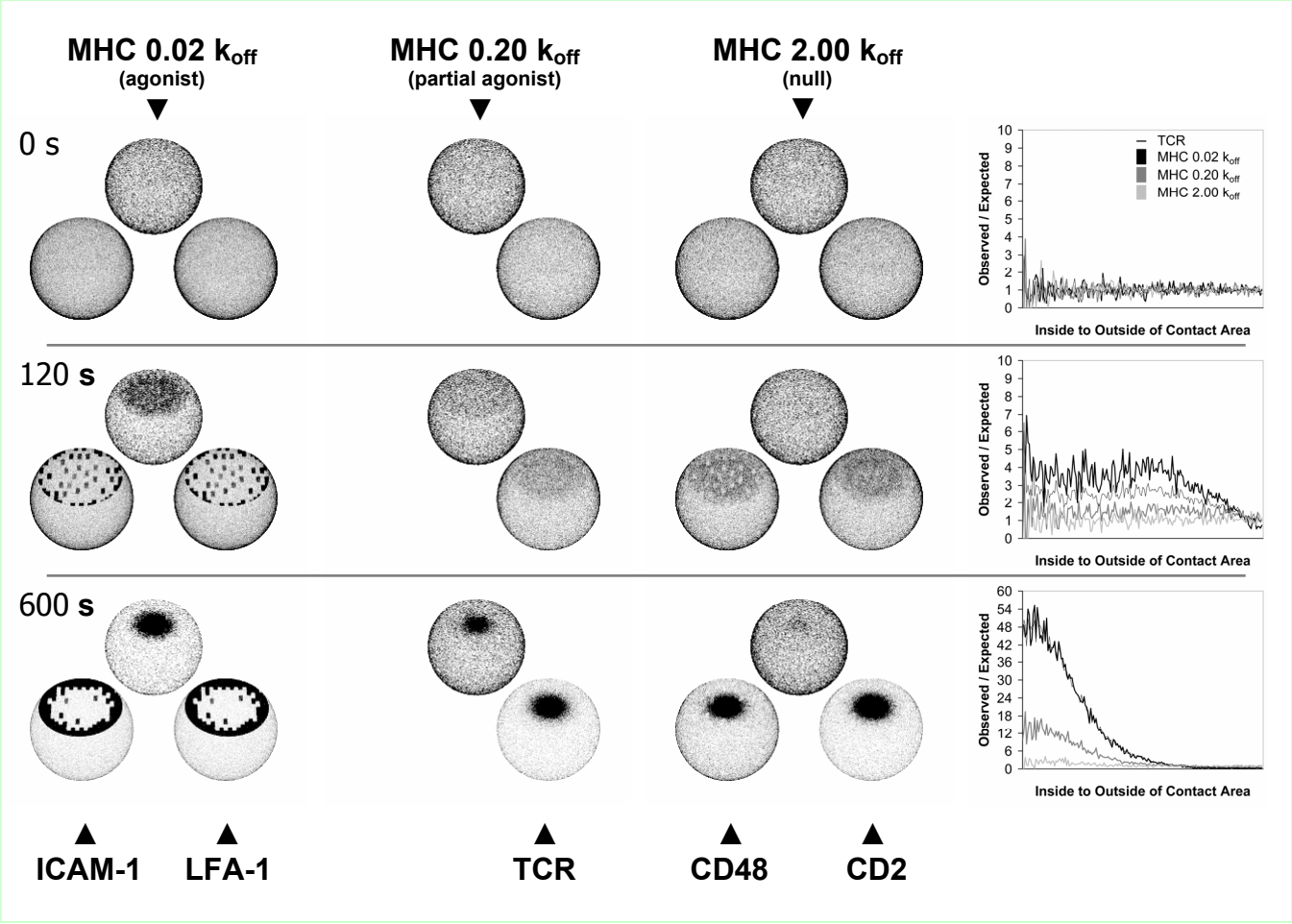
MHC 0.02 koff
(agonist)
MHC 0.20 koff
(partial agonist)
MHC 2.00 koff
(null)
0 s
120 s
600 s
TCR
MHC 0.02 koff
MHC 0.20 koff
MHC 2.00 koff
Observed / Expected
Inside to Outside of Contact Area
ICAM-1
LFA-1
TCR
CD48
CD2

Figure 6

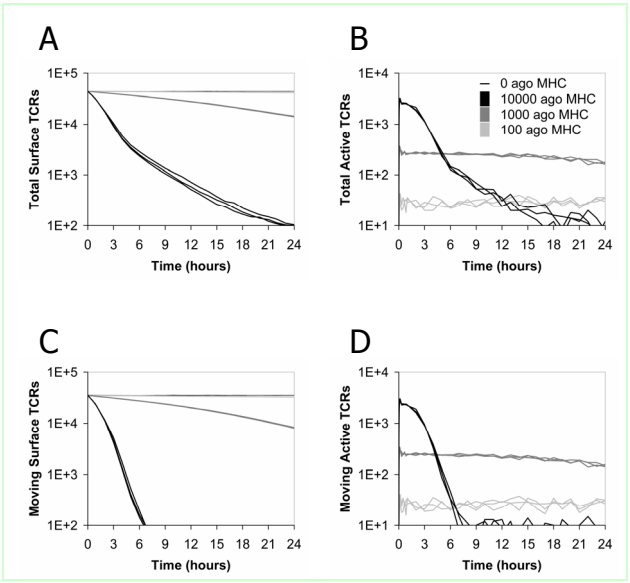
A
B
C
D
Total Surface TCRs
Total Active TCRs
Moving Surface TCRs
Moving Active TCRs
Time (hours)
0 ago MHC
10000 ago MHC
1000 ago MHC
100 ago MHC